ISSN 1075-7015, Geology of Ore Deposits, 2015, Vol. 57, No. 8, pp. 721–731. © Pleiades Publishing, Ltd., 2015.
Original Russian Text © N.V. Chukanov, S.M. Aksenov, R.K. Rastsvetaeva, K.V. Van, D.I. Belakovskiy, I.V. Pekov, V.V. Gurzhiy, W. Schüller, B. Ternes, 2015, published in Zapiski Rossiiskogo Mineralogicheskogo Obshchestva, 2015, No. 2, pp. 48–61.

Mendigite, $Mn_2Mn_2MnCa(Si_3O_9)_2$, a New Mineral Species of the Bustamite Group from the Eifel Volcanic Region, Germany[1]

N. V. Chukanov[a], S. M. Aksenov[b], R. K. Rastsvetaeva[b], K. V. Van[c], D. I. Belakovskiy[d], I. V. Pekov[e], V. V. Gurzhiy[f], W. Schüller[g], and B. Ternes[h]

[a] *Institute of Problems of Chemical Physics, Russian Academy of Sciences, Chernogolovka, Moscow oblast, 142432 Russia*
[b] *Institute of Crystallography, Russian Academy of Sciences, Leninsky pr. 59, Moscow, 117333 Russia*
[c] *Institute of Experimental Mineralogy, Russian Academy of Sciences, Chernogolovka, Moscow oblast, 142432 Russia*
[d] *Fersman Mineralogical Museum, Russian Academy of Sciences, Leninsky pr. 18-2, Moscow, 119071 Russia*
[e] *Faculty of Geology, Moscow State University, Moscow, 119991 Russia*
[f] *Faculty of Geology, St. Petersburg State University, Universitskaya nab. 7/9, St Petersburg, 199034 Russia*
[g] *Im Straussenpesch 22, 53518 Adenau, Germany*
[h] *Bahnhofstrasse 45, 56727 Mayen, Germany*

Received December 10, 2014

Abstract—A new mineral, mendigite (IMA no. 2014-007), isostructural with bustamite, has been found in the In den Dellen pumice quarry near Mendig, Laacher Lake area, Eifel Mountains, Rhineland-Palatinate (Rheinland-Pfalz), Germany. Associated minerals are sanidine, nosean, rhodonite, tephroite, magnetite, and a pyrochlore-group mineral. Mendigite occurs as clusters of long-prismatic crystals (up to 0.1 × 0.2 × 2.5 mm in size) in cavities within sanidinite. The color is dark brown with a brown streak. Perfect cleavage is parallel to (001). $D_{calc} = 3.56$ g/cm^3. The IR spectrum shows the absence of H_2O and OH groups. Mendigite is biaxial (–), $\alpha = 1.722$ (calc), $\beta = 1.782(5)$, $\gamma = 1.796(5)$, $2V_{meas} = 50(10)°$. The chemical composition (electron microprobe, mean of 4 point analyses, the Mn^{2+}/Mn^{3+} ratio determined from structural data and charge-balance constraints) is as follows (wt %): 0.36 MgO, 10.78 CaO, 37.47 MnO, 2.91 Mn_2O_3, 4.42 Fe_2O_3, 1.08 Al_2O_3, 43.80 SiO_2, total 100.82. The empirical formula is $Mn_{2.00}(Mn_{1.33}Ca_{0.67})(Mn^{2+}_{0.50}Mn^{3+}_{0.28}Fe^{3+}_{0.15}Mg_{0.07})(Ca_{0.80}Mn^{2+}_{0.20})(Si_{5.57}Fe^{3+}_{0.27}Al_{0.16}O_{18})$. The idealized formula is $Mn_2Mn_2MnCa(Si_3O_9)_2$. The crystal structure has been refined for a single crystal. Mendigite is triclinic, space group $P\bar{1}$; the unit-cell parameters are $a = 7.0993(4)$, $b = 7.6370(5)$, $c = 7.7037(4)$ Å, $\alpha = 79.58(1)°$, $\beta = 62.62(1)°$, $\gamma = 76.47(1)°$; $V = 359.29(4)$ Å^3, $Z = 1$. The strongest reflections on the X-ray powder diffraction pattern [d, Å (I, %) (hkl)] are: 3.72 (32) (020), 3.40 (20) (002, 021), 3.199 (25) (012), 3.000 (26), (01$\bar{2}$, 1$\bar{2}$0), 2.885 (100) (221, 2$\bar{1}$1, 1$\bar{2}$1), 2.691 (21) (222, 2$\bar{1}$0), 2.397 (21) (02$\bar{2}$, 21$\bar{1}$, 203, 031), 1.774 (37) (412, 3$\bar{2}$1). The type specimen is deposited in the Fersman Mineralogical Museum, Russian Academy of Sciences, Moscow, registration number 4420/1.

DOI: 10.1134/S1075701515080048

INTRODUCTION

Bustamite is frequently regarded as a mineral related to wollastonite or even as a wollastonite-group member (Ohashi and Finger, 1978; Back, 2014). This convergence is based on similar stoichiometry and conformation of the $(Si_3O_9)_\infty$ chains, or "dreierkette", after Grangeon et al. (2013). However, in terms of the crystal structure, the affinity of these pyroxenoids is not very close.

The crystal structure of bustamite was published for the first time by Peacor and Buerger (1962). Later, Ohashi and Finger (1978) investigated the crystal structures of bustamite and wollastonite varieties different in composition and demonstrated substantial structural distinctions between these minerals. The crystal chemical formula of bustamite studied could be expressed as $M1_2M2_2M3M4(Si_3O_9)_2$, where Mn^{2+} is predominant at sites $M1$ and $M3$, whereas sites $M2$ and $M4$ are dominated by Ca (Peacor and Prewitt, 1963; Ohashi and Finger, 1978).

Corresponding author: N.V. Chukanov. E-mail: chukanov@icp.ac.ru

[1] A new mineral, mendigite, and its name were approved by the Commission on New Minerals, Nomenclature, and Classification of the International Mineralogical Association on May 1, 2014, IMA no. 2014-007.

Fig. 1. Clusters of mendigite crystals on cavity wall within sanidinite. FOV 2.8 mm. Photo by S. Wolfsried.

The new mineral, mendigite, described in this article is isostructural with bustamite, but differs in cation arrangement of structural sites. This mineral is named after its type locality near the town of Mendig in the Laacher Lake area, Eifel volcanic region, Rhineland–Palatinate (Rheinland–Pfalz), Germany.

The type specimen is deposited in the Fersman Mineralogical Museum, Russian Academy of Sciences, Moscow, registration number 4420/1.

OCCURRENCE

The fragment of cavernous sanidinite with mendigite was found in the operating pumice quarry In den Dellen near the town of Mendig. The new mineral was found in a postmagmatic (probably pneumatolitic) paragenetic assemblage consisting of sanidine, nosean, rhodonite, tephroite, magnetite, and a pyrochlore group mineral. Crystals of these minerals occur in small miarolitic cavities within nearly monomineralic sanidinite.

Chukanov et al. (2014) discussed in detail the formation conditions of nosean-bearing sanidinite and related complex of various manganese minerals in the Laacher Lake area. Some researchers regard sanidinite as host metamorphic rock deeply altered at high K activity, whereas others workers regard it as a magmatic rock cogenetic to parental phonolite magma. In any case, host metamorphic rocks are the most probable source for Mn. In particular, this is indicated by striation (interpreted as a result of primary stratification) that is occasionally observed in the contact zone of sanidinite-containing miarolitic cavities with Mn minerals.

MORPHOLOGY AND PHYSICAL PROPERTIES

Mendigite occurs as imperfect long-prismatic crystals up to 0.1 × 0.2 × 2.5 mm in size (Fig. 1) flattened on {001}. Some crystals are polysynthetic twins parallel to (100); the constituents of twins are linked by the transfer matrix [100/½$\bar{1}$0/101].

The mineral is dark brown with a brown streak and strong vitreous luster. Perfect cleavage is parallel to (001). The calculated density is 3.56 g/cm^3.

Mendigite is optically biaxial negative, $\beta = 1.782(5)$, $\gamma = 1.796(5)$, $2V = 50(10)°$. Due to a perfect cleavage, the measurement of α failed. The value estimated from average values of β, γ and $2V$ is 1.722. The dispersion of optical axes is medium, $r > v$. The mineral is not pleochroic. The extinction angle is about 4–5° relative to the crystal elongation (i.e., relative to [100]).

The IR spectrum of the mendigite powdery sample prepared as a pellet pressed with KBr (Fig. 2a) was measured using an ALPHA FTIR spectrometer, Bruker Optics, within the wavenumber range 360–3800 cm^{-1}, at a resolution of 4 cm^{-1}, and 16 scans. A pure KBr disc was used as a reference.

The position (cm^{-1}) and assignment of the bands in the IR spectrum of mendigite are as follows (s is strong band, sh is shoulder): 1088s, 1030s, 945s, 907s (Si–O stretching vibrations), 694, 655, 564 (O–Si–O bending vibrations), 515, 461s, 445, 425sh (lattice modes involving Si–O–Si bending and M···O stretching vibrations, where M = Mn, Fe, Ca). Bands corresponding to H-, B- and C-bearing groups are absent in the IR spectrum of mendigite. The IR spectrum of mendigite is close to that bustamite (Fig, 2b); as com-

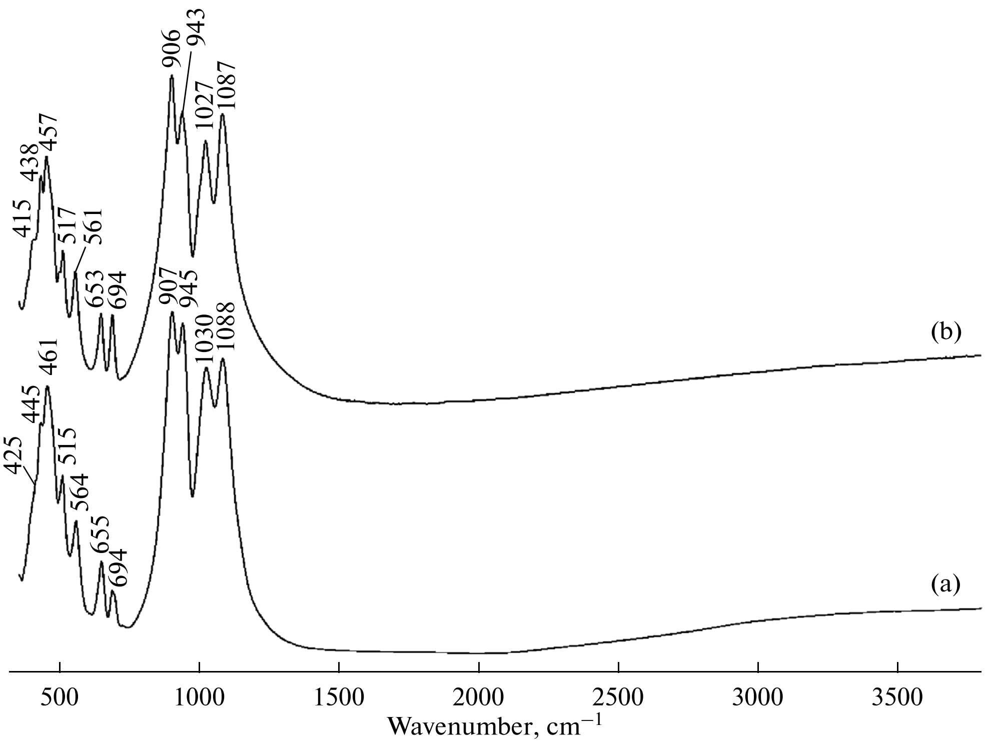

Fig. 2. IR spectra of (a) mendigite and (b) bustamite from Broken Hill, New South Wales, Australia.

pared with the latter, it is characterized by the high-frequency shifts of the most bands.

CHEMICAL COMPOSITION

The chemical composition of mendigite was determined on a Tescan Vega II XMU scanning electron microscope equipped with an INCAx-sight EDS operating on tungsten cathode at an accelerating voltage of 15.7 kV. The current of the absorbed electrons on Co was 0.5 nA. The take-off angle of X-ray radiation was 35°, and the focal distance between sample and detector was 25 mm.

The chemical composition (wt %) is given in Table 1. The empirical formula of mendigite calculated on the basis of 12 (Mg + Ca + Mn + Al + Fe + Si) atoms is $(Ca_{1.47}Mn^{2+}_{4.03}Mg_{0.07}Mg^{3+}_{0.28}Fe^{3+}_{0.15})_{6.00}$ $[(Si_{5.57}Fe^{3+}_{0.27}Al_{0.16})_{\Sigma 6.00}O_{18}]$. Taking into acount structural data (see below), this formula could written as $Mn_{2.00}(Mn_{1.33}Ca_{0.67})(Mn^{2+}_{0.50}Mg^{3+}_{0.28}Fe^{3+}_{0.15}Mg_{0.07})(Ca_{0.80}Mn^{2+}_{0.20})(Si_{5.57}Fe^{3+}_{0.27}Al_{0.16}O_{18})$.

Al and a part of Fe^{3+} are placed in tetrahedral sites to the total of tetrahedral cations equal to 6. Based on the charge–balance constraints for the bulk formula, trivalent state is accepted for all Fe at the octahedral sites and for a part of Mn (0.28 Mn^{3+} apfu). Substantial Fe^{3+} and Mn^{3+} contents are confirmed by very high refractive indices as compared to bustamite and by a good compatibility of physical properties and chemical composition calculated from the Gladstone–Dale equation $(1 - K_p/K_c) = -0.037$ ("excellent"), whereas the assumption of a bivalent state for all Fe and/or Mn would result in poor compatibility.

The idealized formula of mendigite is $Mn_2Mn_2MnCa(Si_3O_9)_2$.

Table 1. Chemical composition of mendigite (average of 4 point analyses)

Component	Content, wt %	Range	Standard
MgO	0.36	0.25–0.49	Diopside
CaO	10.78	10.11–10.92	Wollastonite
MnO*	37.47	39.37–40.80**	$MnTiO_3$
Mn_2O_3*	2.91		
Fe_2O_3	4.42	4.15–4.70	Fe_2O_3
Al_2O_3	1.08	0.87–1.28	Albite
SiO_2	43.80	43.24–44.54	SiO_2
Total	100.82		

* Total manganese (corresponding to 40.09 wt % MnO) was apportioned between MnO and Mn_2O_3 taking into account structural data and charge balance constraints in the empirical formula.

** For total manganese calculated as MnO.

Table 2. Powder X-ray diffraction data for mendigite

I_{meas}	d_{meas}	I_{calc}*	d_{calc}**	*hkl*
8	4.84	13	4.813	$01\bar{1}$
12	4.40	10	4.397	$1\bar{1}0$
32	3.72	27	3.699	020
20	3.40	32, 5	3.408, 3.373	002, 021
25	3.199	47	3.200	012
26	3.000	47, 5	3.000, 2.961	$01\bar{2}$, $1\bar{2}0$
100	2.885	100. 92, 5	2.883, 2.879, 2.867	221, $2\bar{1}1$, $1\bar{2}1$
21	2.691	4, 7	2.703, 2.701	222, 210
12	2.622	16	2.620	022
13	2.464	18, 7, 7	2.466, 2.450, 2.449	030, $20\bar{1}$, 213
21	2.397	10, 11, 14, 1	2.407, 2.403, 2.400, 2.385	$02\bar{2}$, $21\bar{1}$, 203, 031
13	2.272	8, 1, 2, 11, 2, 3, 2	2.275, 2.273, 2.272, 2.271, 2.259, 2.256, 2.256	231, $1\bar{1}3$, 003, $2\bar{2}1$, $03\bar{1}$, 223, $2\overline{11}$
17	2.227	29	2.226	013
18	2.112	19, 17	2.117, 2.113	230, $2\bar{2}2$
37	1.774	34, 2	1.775, 1.773	412, $3\bar{2}1$
10	1.703	20	1.704	004
19	1.659	11, 11, 9, 8	1.662, 1.662, 1.654, 1.653	234, $2\overline{22}$, 243, $2\overline{31}$
14	1.554	7, 7, 4, 6	1.558, 1.555, 1.552, 1.552	$24\bar{1}$, $2\bar{3}3$, 400, 424
5	1.480	3, 4, 3	1.482, 1.481, 1.480	252, $2\bar{4}0$, 050
4	1.427	2, 3	1.430, 1.427	430, $4\bar{1}4$
3	1.349	1, 1, 4	1.352, 1.351, 1.349	444, $4\bar{2}0$, $03\bar{4}$
6	1.318	2, 7	1.322, 1.317	$2\bar{2}5$, $05\bar{2}$
3	1.291	1, 3, 1, 1	1.293, 1.291, 1.291, 1.290	$5\bar{1}3$, 053, 245, $2\overline{33}$
2	1.232	4, 5, 5	1.232, 1.230, 1.229	061, $41\bar{2}$, 416

* Only reflections with intensities ≥1 are given.
** Calculated from single-crystal data.

X-RAY CRYSTALLOGRAPHY

The powder X-ray diffraction data of mendigite (Table 2) were collected using an Agilent Technologies Super-Nova diffractometer with an Atlas CCD detector operating at CuK_α radiation (microfocusing instrument was used), accelerating voltage 50 kV, and current intensity 0.8 mA. The experiment has been carried out using the Gandolfi method; the distance between sample and detector was 55 mm. All reflections of the mineral X-ray diffraction pattern are indexed in the triclinic cell with the following unit-cell parameters refined from the powder data: $a = 7.11(2)$, $b = 7.65(2)$, $c = 7.70(2)$ Å, $\alpha = 79.54(8)°$, $\beta = 62.65(8)°$, $\gamma = 76.32(9)°$, $V = 359.8(7)$ Å^3.

Single-crystal X-ray data were collected in a full sphere of reciprocal space on an Xcalibur Oxford Diffraction CCD diffractometer (MoK_α radiation). The calculated triclinic unit cell parameters (space group $P\bar{1}$) are as follows: $a = 7.0993(4)$, $b = 7.6370(5)$, $c = 7.7037(4)$ Å, $\alpha = 79.58(1)°$, $\beta = 62.62(1)°$, $\gamma = 76.47(1)°$, $V = 359.29(4)$ Å^3, $Z = 1$. The transition from primitive unit cell with $a = 7.0993(4)$, $b = 7.6370(5)$, $c = 7.7037(4)$ Å, $\alpha = 79.58(1)°$, $\beta = 62.62(1)°$, $\gamma = 76.47(1)°$ (space group $P\bar{1}$) to the body-

Table 3. Crystallographic data and refinement details for mendigite

Formula	$Mn_2(Mn_{1.33}Ca_{0.67})(Mn_{0.78}Fe_{0.15}Mg_{0.07})(Ca_{0.8}Mn_{0.2})(Si_3O_9)_2$
Absorption, μ, mm^{-1}	5.24
Density, D_x, g/cm^3	3.56
Space group	$P\bar{1}$
a (Å)	7.0993(4)
b (Å)	7.6370(5)
c (Å)	7.7037(4)
α (°)	79.58(1)
β (°)	62.62(1)
γ (°)	76.47(1)
V ($Å^3$)	359.29(4)
Crystal size, mm	0.75 × 0.05 × 0.05
Diffractometer	Xcalibur Oxford Diffraction (CCD-detector)
Radiation; wavelength, Å	MoK_{α}, 0.7107
Data collection method	ω
Temperature, K	293
$F(000)$	373
θ range for data, degree	4.23—56.11
Index ranges *h*, *k*, *l*	$-9 < h < 15$, $-17 < k < 17$, $-17 < l < 17$
Total reflections	19616
Number of unique reflections	7567
Number of unique reflectons with $I > 3\sigma(I)$	4144
R value of averaged equivalent reflections	8.03
Refinement method	Full-matrix least-squares on *F*, with weights $w = 1/(\sigma^2 F + 0.0016F^2)$
GOF	1.06
R_1/wR_2 (%)	0.0559/0.091
$\Delta\rho_{min}/\Delta\rho_{max}$	−2.35/1.86
Calculation programs	Jana2006, AREN

$R_1 = \Sigma||F_{obs}| - |F_{calc}||/\Sigma|F_{obs}|$, $wR_2 = \left\{\Sigma[w(F^2_{obs} - F^2_{calc})^2]/\Sigma[w(F^2_{obs})^2]\right\}^{1/2}$, $GOF = \{\Sigma[w(F^2_{obs} - F^2_{calc})]/(n-p)\}^{1/2}$, where *n* is number of reflections, *p* is number of refined parameters

Table 4. Atom coordinates, repetition factor of sites (Q) and isotropic displacement parameters (U_{eq}) for the crystal structure of mendigite

Site	x	y	z	Q	Ueq
$M1$	−0.0501(1)	0.2049(1)	0.2530(1)	2i	0.0105(1)
$M2$	−0.4364(1)	0.7963(1)	0.7518(1)	2i	0.0138(1)
$M3$	0	0.5	0.5	1g	0.0078(1)
$M4$	0.5	0.5	0.5	1h	0.0065(2)
Si1	−0.2458(1)	0.8263(1)	0.2710(1)	2i	0.0060(2)
Si2	−0.3157(1)	0.1755(1)	0.7384(1)	2i	0.0058(2)
Si3	0.2001(1)	0.6053(1)	0.0408(1)	2i	0.0060(2)
O1	0.0060(2)	0.4298(2)	0.1954(2)	2i	0.0092(5)
O2	−0.1979(5)	0.2990(3)	0.5418(3)	2i	0.0165(7)
O3	−0.0312(3)	0.7445(3)	0.0793(3)	2i	0.0119(5)
O4	0.3152(4)	0.5931(2)	−0.1916(2)	2i	0.0106(5)
O5	−0.2191(6)	0.9648(3)	0.7464(4)	2i	0.0218(9)
O6	−0.2615(5)	0.6914(3)	0.4645(3)	2i	0.0147(6)
O7	0.3430(4)	0.7301(3)	0.0729(3)	2i	0.0117(6)
O8	−0.2665(6)	0.0346(3)	0.2910(4)	2i	0.0219(8)
O9	−0.4415(5)	0.8079(7)	0.2276(5)	2i	0.044(2)

U_{eq} is defined as one third of the orthogonalized U_{ij} tensor trace.

centered unit cell proposed by Ohashi and Finger (1978) may be realized using the matrix $[0\bar{1}1/1\overline{11}/\bar{1}00]$.

The structure was determined with the "charge flipping" procedure using the SUPERFLIP program (Palatinus and Chapuis, 2007). Because of the complex chemical composition, cation distribution through the structural sites was performed based on crystal chemical criteria taking into account displacement parameters, interatomic distances, ionic radii of the cations, and controlling R values. The mixed curves of atomic scattering were used for a number of sites. The model was refined to final $R = 5.59\%$ using 4144 unique reflections with $I > I\sigma(I)$ in the anisotropic approximation taking into account the twinning (twinning matrix $[100/\frac{1}{2}\bar{1}0/20/101]$, the ratio of two twin components 0.6 : 0.4). All calculations were performed with the JANA2006 (Petricek et al., 2006) and AREN (Andrianov, 1987) crystallographic software packages.

The crystallographic data, details of single-crystal experiment, and results of the mendigite structural analysis are given in Tables 3–6.

Mendigite is isostructural with bustamite and ferrobustamite. The crystal structure of these minerals, which may be combined into the bustamite group, is based on triple-row bands of M cations and wollastonite-type chains of SiO_4 tetrahedra (Figs. 3–5).

The following distribution of cations by sites M (assumed cation assignment is given in brackets taking into account the electron microprobe data) was obtained as a result of refinement taking into account the cation–oxygen distances: $M1$ – only Mn^{2+} [Mn^{2+}]; $M2$ – Mn^{2+} with minor Ca [$Mn^{2+}_{1.33}Ca_{0.67}$];

Table 5. Anisotropic displacement parameters (Å^2) for mendigite

Site	U_{11}	U_{22}	U_{33}	U_{12}	U_{13}	U_{23}
*M*1	0.0113(2)	0.0098(1)	0.0095(1)	0.0001(1)	–0.0042(1)	–0.0018(1)
*M*2	0.0099(2)	0.0171(2)	0.0107(1)	–0.0034(1)	–0.0007(1)	–0.0020(1)
*M*3	0.0068(2)	0.0089(1)	0.0076(1)	–0.0029(2)	–0.0025(2)	–0.0006(1)
*M*4	0.0033(2)	0.0097(2)	0.0076(2)	–0.0018(2)	–0.0022(2)	–0.0031(1)
Si1	0.0024(2)	0.0074(2)	0.0077(2)	–0.0016(2)	–0.0017(2)	0.0002(2)
Si2	0.0041(3)	0.0069(2)	0.0068(2)	–0.0020(2)	–0.0023(2)	–0.0003(2)
Si3	0.0041(3)	0.0080(2)	0.0052(2)	–0.0020(2)	–0.0014(2)	0.0003(1)
O1	0.0104(8)	0.0069(4)	0.0076(4)	–0.0022(5)	–0.0019(5)	0.0012(3)
O2	0.028(1)	0.0130(6)	0.0073(5)	–0.0132(8)	–0.0025(7)	0.0011(5)
O3	0.0045(7)	0.0138(7)	0.0105(6)	0.0026(5)	0.0000(5)	0.0007(5)
O4	0.0106(8)	0.0104(5)	0.0074(5)	–0.0031(6)	–0.0004(6)	–0.0010(4)
O5	0.031(2)	0.0100(6)	0.0207(9)	0.0086(8)	–0.014(1)	–0.0020(6)
O6	0.0131(9)	0.0127(6)	0.0092(5)	0.0016(6)	–0.0002(6)	0.0032(4)
O7	0.0152(9)	0.0164(7)	0.0074(5)	–0.0093(6)	–0.0053(5)	–0.0006(5)
O8	0.024(1)	0.0100(6)	0.0208(8)	–0.0078(8)	0.0024(9)	–0.0033(6)
O9	0.009(1)	0.096(3)	0.037(2)	–0.008(2)	–0.009(1)	–0.037(2)

Table 6. Selected interatomic distances (Å) in mendigite

*M*1	O5	2.045(4)	*M*4	O4	2.276(1) × 2
	O8	2.126(4)		O6	2.380(3) × 2
	O2	2.156(2)		O2	2.444(3) × 2
	O4	2.311(2)		O9	2.824(4) × 2
	O3	2.328(2)		Average	2.481
	O1	2.412(3)			
	Average	2.230			
*M*2	O6	2.175(2)	Si1	O8	1.592(3)
	O5	2.211(4)		O9	1.612(5)
	O7	2.211(4)		O6	1.625(2)
	O8	2.332(4)		O3	1.647(2)
	O1	2.401(2)		Average	1.619
	O4	2.457(3)			
	Average	2.309			
*M*3	O6	2.170(3) × 2	Si_2	O5	1.597(2)
	O1	2.192(1) × 2		O9	1.597(4)
	O2	2.202(3) × 2		O2	1.603(2)
	Average	2.188		O7	1.650(3)
				Average	1.612
			Si_3	O4	1.600(2)
				O1	1.607(2)
				O3	1.663(2)
				O7	1.663(3)
				Average	1.633

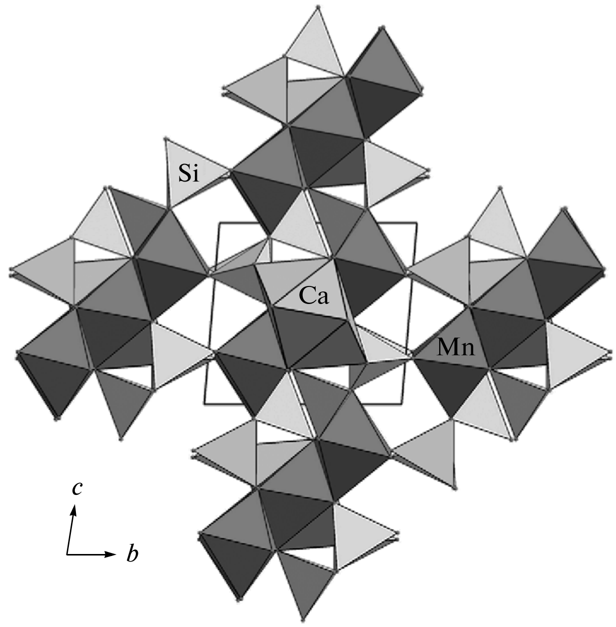

Fig. 3. Crystal structure of mendigite projected on (100) plane.

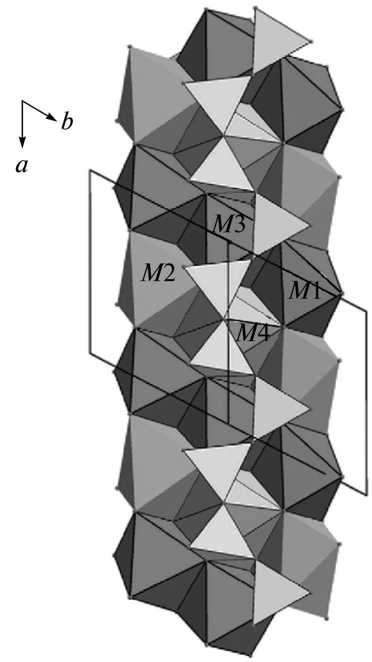

Fig. 4. Triple-row band of mendigite formed by *M*1–*M*4 polyhedra.

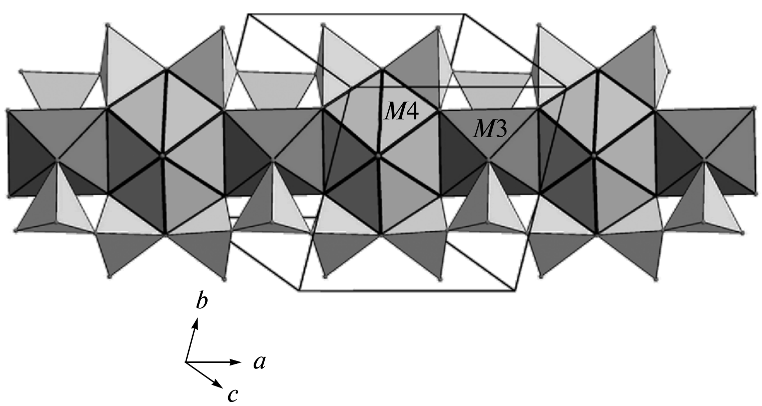

Fig. 5. Silicate chains in mendigite and their linkage to the octahedral band.

*M*3 – Mn^{2+} with minor Mn^{3+}, Fe^{3+}, and Mg [$Mn^{2+}_{0.50}Mn^{3+}_{0.28}Fe^{3+}_{0.15}Mg_{0.07}$]; and *M*4 – Ca with admixture of Mn^{2+} [$Ca_{0.80}Mn^{2+}_{0.20}$].

DISCUSSION

The major difference between the structural types of bustamite and wollastonite is the linkage of tetrahedral chains to the system of *M*-polyhedra (Peacor and Prewitt, 1963; Ohashi and Finger, 1978; Angel, 1985, 1986). This difference is illustrated in Fig. 6.

The structural type of bustamite is characterized by four cation sites *M*1, *M*2, *M*3, and *M*4 with coordination numbers 6, 6, 6, and 6 + 2, respectively (in the polyhedron *M*4, two cation–oxygen distances are substantially longer than the other six cation–oxygen distances). In wollastonite-type structure only three cation sites *M*1, *M*2, and *M*3 with coordination numbers 6, 6, and 7, respectively, are present.

The bustamite group members differ in the arrangement of cations at *M*-sites. In ferrobustamite, $Ca_2Ca_2FeCa(Si_3O_9)_2$ (Burnham, 1975; Yamanaka et al., 1977) Fe^{2+} is predominant in the small *M*3 octahedron, whereas at the other *M* sites, Ca is predominant. Bustamite, $Mn_2Ca_2MnCa(Si_3O_9)_2$ and mendigite $Mn_2Mn_2MnCa(Si_3O_9)_2$ differ in cation predominant at the site *M*2 (Ca and Mn^{2+}, respectively). The

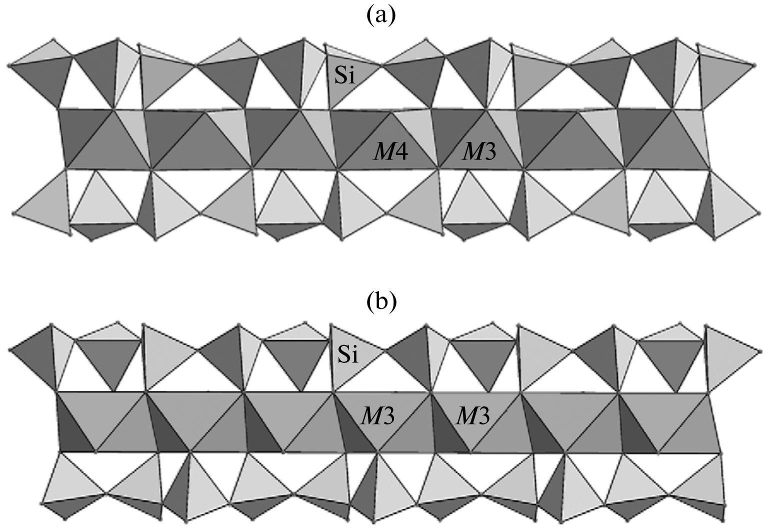

Fig. 6. Linkage of wollastonite-type silicate chains to octahedral bands in the crystal structures of (a) bustamite and (b) wollastonite.

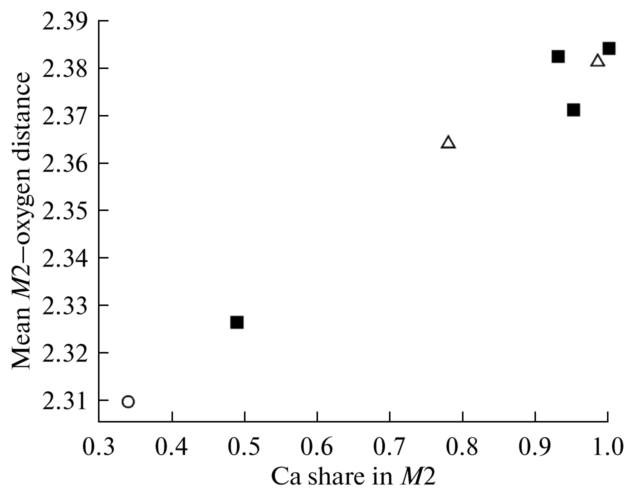

Fig. 7. Correlation between mean *M*2–oxygen distance and fractional Ca content at *M*2 site. Squares correspond to bustamite and "manganoan bustamite" (Peacor and Buerger, 1962; Ohashi and Finger, 1978); triangles correspond to ferrobustamite (Rapoport and Burnham, 1973; Yamanaka et al., 1977), and circle corresponds to mendigite.

predominance of Mn over Ca at the site *M*2 in mendigite is supported by the average distance *M*2–O. As follows from correlation between this value and a fraction of Ca at the *M*2 site obtained by means of X-ray structural analysis (Fig. 7), the Mn^{2+}/Ca ratio at site *M*2 of mendigite is close to 2.

As is seen from available compositional data for minerals with a bustamite-type structure (Mason, 1975; Ohashi and Finger, 1978; Minerals, 1981), mendigite is extremely rare in nature. In addition to the holotype sample described in this paper, only one natural sample is known, for which the insignificant predominance of Mn over Ca at the site *M*2 (Mn^{2+} : Ca = 51 : 49) could be assumed. It comes from a lens of manganese ore hosted in dolomite marble of the Mitsuka deposit, Japan (Ohashi and Finger, 1978).

Comparative data for mendigite and related minerals are given in Table 7. It should be emphasized that the new mineral substantially differs from bustamite and ferrobustamite in optical parameters and density.

ACKNOWLEDGMENTS

This study was supported by the Russian Science Foundation (project no. 14-17-00048) with regard to mineralogical investigations, and Russian Foundation

Table 7. Comparative data for bustamite–mendigite group members, bustamite and ferrobustamite

Mineral	Mendigite	Bustamite	Ferrobustamite
Formula	$Mn_2Mn_2MnCa(Si_3O_9)_2$	$Mn_2Ca_2MnCa(Si_3O_9)_2$	$Ca_2Ca_2FeCa(Si_3O_9)_2$
Simplified formula	$Mn_5Ca(Si_3O_9)_2$	$Mn_3Ca_3(Si_3O_9)_2$	$Ca_5Fe\ (Si_3O_9)_2$
Symmetry	Triclinic, $P\bar{1}$	Triclinic, $P\bar{1}$	Triclinic, $P\bar{1}$
a, Å	7.0993	7.139	7.253
b, Å	7.6370	7.719	7.862
c, Å	7.7037	7.747	7.900
α, °	79.58	79.257	79.23
β, °	62.62	63.074	62.117
γ, °	76.47	76.175	76.710
V, Å^3	359.3	368.0	385.9
Z	1	1	1
Strong lines of the powder X-ray: *d*, Å (*I*, %)	3.72 (32) 3.40 (20) 3.199 (25) 3.000 (26) 2.885 (100) 2.691 (21) 2.397 (21) 1.774 (37)	3.19 (50) 2.989 (60) 2.880 (100) 2.711 (30) 2.227 (40) 1.776 (50) 1.665 (40)	7.67 (25) 3.84 (55) 3.470 (60) 3.270 (100) 3.049 (80) 2.696 (30) 2.278 (65)
Optical data:			
α	1.722 (calc.)	1.640–1.695	1.640
β	1.782	1.651–1.708	No data
γ	1.796	1.680–1.710	1.653
Optical sign, 2*V*, °	–50	–(34–60)	–60
Density, g/cm^3	3.56	3.32–3.46	3.09
Source	This study	Ohashi, Finger, 1978; Deer et al., 1978; Harada et al., 1974; Minerals (1981)	Deer et al., 1978; Yamanaka et al., 1977; Rapoport, Burnham, 1973; Shimazaki, Tanaka, 1973; Minerals (1981)

Unit-cell parameters are given in the unified orientation accepted in this work. Unit-cell parameters given for bustamite by Ohashi and Finger (1978) are $a = 9.864$, $b = 10.790$, $c = 7.139$ Å, $\alpha = 99.53$, $\beta = 99.71$, $\gamma = 83.83°$. Matrix of transition to new cell is [0 0 –1, –½ –½ –½, ½ –½ –½]. Unit-cell parameters of ferrobustamite published by Yamanaka et al. (1977) are: $a = 7.862$, $b = 7.253$, $c = 13.967$ Å, $\alpha = 89.44$, $\beta = 95.28$, $\gamma = 103.29°$. The corresponding transition matrix is [0 –1 0, 1 0 0, 0 –½ –½].

for Basic Research (project no. 14-05-00190) and Council for Grants of the President of the Russian Federation (project MK-4990.2014.5) with regard to crystal chemical investigation.

REFERENCES

Andrianov, V.I., Development of the system of crystallographic programs RENTGEN for the computers NORD, SM-4 and US, *Kristallografiya,* 1987, vol. 32, pp. 228–231.

Angel, R.J. Structural variation in wollastonite and bustamite, *Mineral. Mag.*, 1985, vol. 49, pp. 37–48.

Angel, R.J., Transformation mechanisms between single-chain silicates, *Am. Mineral.*, 1986, vol. 71, pp. 1441–1454.

Brown, I.D. and Altermatt, D. Bond-valence parameters obtained from a systematic analysis of the Inorganic Crystal Structure Database, *Acta Crystallogr.*, 1985, vol. 41, pp. 244–247.

Burnham, C.W., Ferrobustamite: the crystal structures of two Ca, Fe bustamite-type pyroxenoids: correction, *Z. Kristallogr.*, 1975, vol. 142, pp. 450–452.

Chukanov, N.V., Krivovichev, S.V., Pakhomova, A.S., Pekov, I.V., Schäfer, Ch., Vigasina, M.F., and Van, K.V., Laachite $(Ca,Mn)_2Zr_2Nb_2TiFeO_{14}$, a new zirconolite-related mineral from the Eifel volcanic region, Germany, *Eur. J. Mineral.*, 2014, vol. 26, pp. 103–111.

CrysAlisPro, Agilent Technologies, version 1.171.36.20 (ed. 27-06-2012).

Deer, W.A., Howie, R.A., and Zussman, J., *Rock-Forming Minerals. Vol 2A: Single-Chain Silicates*, London: Longman, 1978.

Grangeon, S., Claret, F., Lerouge, C., Warmont, F., Sato, T., Anraku, S., Numako, C., Linard Y., and Lan-son, B., On the nature of structural disorder in calcium silicate hydrates with a calcium/silicon ratio similar to tobermorite, *Cem. Concr. Res.*, 2013, vol. 52., pp. 31–37.

Harada, K., Sekino, H., Nagashima, K., Watanabe,T., and Momoi H., High-iron bustamite and fluorapatite from the Broken Hill mine, New South Wales, Australia, *Mineral. Mag.*, 1974, vol. 39, pp. 601–604.

Mason, B., Compositional limits of wollastonite and bustamite., *Am. Mineral.*, 1975, vol. 60, pp. 209–212.

Mineraly. Sparovochnik (Minerals. Reference Book) Chukhrov, F.V. and Smolyaninova, N.N., Eds. Moscow: Nauka, 1981, vol. III, pt. 2.

Ohashi, Y. and Finger, L.W., The role of octahedral cations in pyroxenoid crystal chemistry. I. Bustamite, wollastonite, and pectolite–schizolite–serandite series, *Am. Mineral.*, 1978, vol. 63, pp. 274–288.

Palatinus, L. and Chapuis G. SUPERFLIP – a computer program for the solution of crystal structures by charge flipping in arbitrary dimensions, *J. Appl. Cryst.*, 2007, vol. 40, pp. 786–790.

Peacor, D.R. and Buerger, M.J., Determination and refinement of the crystal structure of bustamite, $CaMnSi_2O_6$, *Z. Kristallogr.*, 1962, vol. 117, pp. 331–343.

Peacor, D. R. and Prewitt, M.J., Comparison of the crystal structures of bustamite and wollastonite, *Am. Mineral.*, 1963, vol. 48. pp. 588–596.

Petricek, V., Dužek, M., and Palatinus, L., *Jana 2006. Structure Determination Software Programs*, Praha, Institute of Physics, 2006.

Shimazaki, H. and Yamanaka, T., Iron-wollastonite from skarns and its stability relation in the $CaSiO_3$–$CaFeSi_2O_6$ join, *Geochem. J.*, 1973, vol. 7, pp. 67–79.

Yamanaka, T., Sadanaga, R., Takeuchi, Y., Structural variation in the ferrobustamite solid solution, *Am. Mineral.*, 1977, vol. 62, pp. 1216–1224.

Translated by I. Baksheev